J. Fluid Mech. (1986), *vol.* 173, *pp.* 253–272
Printed in Great Britain

Convective flows with multiple spatial periodicities

By MARY LOWE†, B. STEVEN ALBERT AND J. P. GOLLUB
Physics Department, Haverford College, Haverford, PA 19041, USA *and* Physics Department, the University of Pennsylvania, Philadelphia, PA 19104, USA

(Received 25 March 1986)

The response of a convective flow to spatially periodic forcing at a period different from the critical wavelength is investigated experimentally. For reasons of experimental convenience, we utilize an electrohydrodynamic instability in a thin layer of nematic liquid. With this system, a sample containing several hundred rolls is easily obtained, and periodic forcing is imposed electrically using a specially designed interdigitated electrode. Several novel flows with multiple periodicities are found. They may be broadly classified as commensurate (phase-locked) or incommensurate (quasi-periodic) flows, depending on whether the dominant periodicity of the perturbed flow and the periodicity of the forcing are in the ratio of small integers. Near the instability threshold and for weak forcing, an approximation of slow spatial variations is satisfied. In that case, the flows can be described quantitatively by an amplitude equation. We note a close connection between these hydrodynamic phenomena and a problem of competing periodicities that occurs in statistical mechanics. This relationship leads us to suggest the use of a discontinuous function for describing certain incommensurate flows in which non-repeating short and long groups of rolls are observed to occur in an irregular sequence. We also note, as predicted by Pal & Kelly, that two-dimensional forcing can lead to a three-dimensional flow.

1. Introduction

Many of the simplest hydrodynamic instabilities yield spatially periodic flows that break the translational symmetry of the system. The rolls that occur in Taylor–Couette flow and Rayleigh–Bénard convection are good examples. In this paper, we address the question of how the flows resulting from these instabilities are modified when the symmetry of the system is broken by an *imposed* spatially periodic forcing at a wavenumber that may differ from the critical wavenumber of the instability. We shall sometimes refer to this as a problem of competing periodicities.

This question was first raised theoretically by Kelly & Pal a few years ago in the context of thermal convection (Kelly & Pal 1978; Pal & Kelly 1978, 1979). They carefully considered the immediate region of the transition and showed that, for certain forcing periodicities, the sharp bifurcation is replaced by a smooth (imperfect) one. They also showed that two-dimensional thermal forcing can lead to three-dimensional flow.

There has been little experimental work on the problem of competing periodicities near instability thresholds. (However, periodic forcing has been used to create flows with a desired predetermined wavenumber; see Chen & Whitehead 1968; Busse &

† Current address: Group P-10, MS-K764, Los Alamos National Laboratory, Los Alamos, NM 87545, USA.

Whitehead 1971.) One reason may be that the phenomena are subtle and easily masked by finite-size effects. For example, a convective flow containing ten rolls would clearly be too small to exhibit the phenomena of interest adequately.

In this paper, we utilize an electrohydrodynamic (EHD) instability that leads to convection in a thin fluid layer of nematic liquid crystal less than 200 μm thick. This system has many advantages for studying competing periodicities. First, stable convective flows with hundreds of two-dimensional rolls can easily be produced; finite-size effects are largely eliminated. Secondly, the anisotropy of the fluid can be used to stabilize the pattern against three-dimensional perturbations, so that the phenomena of competing periodicities become largely two-dimensional. Thirdly, the flow can be forced at a precisely defined wavenumber with an easily controlled amplitude using a photolithographically etched electrode. The ratio between the forcing periodicity and the natural roll size is continuously adjustable by varying the thickness of the nematic layer. Finally the patterns are easily observed in real space by optical microscopy because the flow produces strong spatial variations in the index of refraction. Digitization of the optical intensity patterns and spatial Fourier analysis allow quantitative analysis of the flows.

A considerable variety of novel (and beautiful) hydrodynamic flows with multiple periodicities were discovered in this investigation. Broadly speaking, they fall into two distinct categories: commensurate flows, which occur when the dominant periodicity of the fluid and the forcing period are in the ratio of small integers; and incommensurate flows, in which this is not the case. The various flows are realized by changing either the roll size of the forcing strength or both.

We find that each of these broad categories can be subdivided into several distinct flows. One particularly interesting incommensurate flow takes the form of a slow phase modulation in which the widths of the convective rolls are not identical. Most of the width variation occurs in narrow regions that can be quantitatively described by solutions to the pendulum equation. A theoretical explanation of these incommensurate flows has recently been developed by Coullet (1986). The explanation essentially depends on only two factors. (i) The system is near threshold so that the flow can be described by an amplitude equation, a one-dimensional partial differential equation involving slow space and time variations of the amplitude of the rolls. (ii) Symmetry considerations uniquely specify an additional term in the amplitude equation that arises from the forcing. The generality of this approach suggests that similar incommensurate states should occur in many other periodically forced hydrodynamic systems.

Distinctly different types of incommensurate ordering occur for other parameter ranges, One of them bears considerable resemblance to one-dimensional incommensurate atomic arrays, known as quasicrystals, found in solid-state physics. In another case, the competing periodicities lead to a three-dimensional flow.

This paper describes the commensurate and incommensurate patterns found in this non-equilibrium system. (A few of the results on incommensurate patterns have been reported elsewhere (Lowe, Gollub & Lubensky 1983; Lowe & Gollub 1985*a*).) We first describe in §2 the experimental configuration including the electrohydrodynamic instability and the experimental apparatus. Relevant theoretical work is presented in §3. Examples of commensurate patterns are shown in §4, and incommensurate states are described in §5. Finally, in §6, we discuss and summarize the data in the context of the theoretical work.

2. Experimental configuration

2.1. *Description of the electrohydrodynamic instability*

Nematic liquid crystals are anisotropic organic fluids composed of rod-shaped molecules whose local mean orientation is described by a 'director field'. Their hydrodynamic behaviour is more complex than that of isotropic fluids because of the coupling between the director and velocity fields.

Many instabilities may develop in nematics; the one of particular interest in this paper occurs in a thin nematic layer (20–200 μm thick) for which the dielectric constants and conductivities parallel to and perpendicular to the director satisfy the following relationships: $\epsilon_\parallel - \epsilon_\perp < 0$ and $\sigma_\parallel - \sigma_\perp > 0$. The instability is produced when a d.c. or low-frequency a.c. voltage across the layer exceeds a critical value that is independent of the layer depth d. The resulting cellular flow resembles Rayleigh–Bénard convection, and the resulting rolls are often called 'Williams domains'. The width of each roll is approximately equal to the layer depth. The circulation period ranges from a few seconds to fractions of a second, depending on d (Penz 1971). Accompanying the flow is a static spatially periodic distortion in the director field; it remains perpendicular to the roll axis, but is tipped out of the plane of the plates by the flow.

The basic physical mechanism of the instability is complex but not hard to appreciate. In the absence of an applied field, the director is aligned parallel to the plates, in a particular orientation specified by surface treatment of the electrodes. When a field is applied, small fluctuations in the local director orientation lead to charge accumulation due to the anisotropic conductivity of the fluid. Destabilization results from a force on the charges by the electric field, causing the fluid to flow. The accompanying viscous torque amplifies the fluctuations. This leads to an instability when the destabilizing torque is larger than the elastic and dielectric torques that suppress the fluctuations in the director orientation. (For a review, see Goossens 1978.)

2.2. *Sample cell*

The experimental configuration consists of a thin layer of nematic liquid crystal (4-methoxybenzylidene-4′-n-butylaniline or MBBA) that fills the gap between two glass plates coated with a transparent conductive material (In_2O_3). One of the conductive films is photolithographically etched to form an interdigitated electrode. A thin convoluted line (15 μm wide) is removed to divide the electrode into two electrically isolated regions, A and B. As shown in figure 1(*a*), this results in a set of 120 interlaced fingers, to which two different voltages, V_A and V_B, may be applied. The other film is grounded (see figure 1*b*). This leads to a spatially periodic electric field with period $l_1 = 200$ μm over a portion of the sample with dimensions 12 mm × 8 mm.

An analytic expression for the potential can be obtained by a Fourier expansion, if the gaps between the fingers are neglected. A diagram of the resulting equipotential and electric-field lines in the region bounded by the two electrodes is shown in figure 2. One period of the forcing, drawn to scale, is exhibited using realistic parameter values given in the caption. The spatially periodic component of the field is relatively small.

To achieve a uniform director orientation in the absence of periodic forcing, the electrodes are treated in one of two ways. The first is the application of a polymer coating followed by gentle unidirectional rubbing with velveteen. The second is a

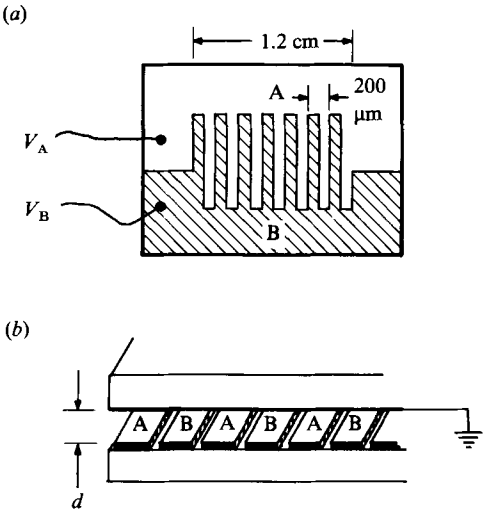

FIGURE 1. Schematic diagram of the interdigitated electrode whose 120 fingers provide a spatially periodic electric field. (*a*) A convoluted line separates the conductive film into two electrically isolated regions, A and B. (*b*) Configuration of the cell.

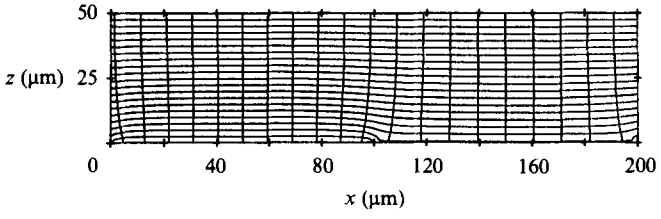

FIGURE 2. One period of the equipotential and electric-field lines over the interdigitated electrode. The layer depth is 50 μm. Two voltages are applied to the lower electrode, located at $z = 0$ μm, with the values $V_A = 6.5$ V for $x < 100$ μm and $V_B = 5.9$ V for $x > 100$ μm.

thin-film evaporation of SiO on to the electrode at oblique incidence (Urbach, Boix & Guyon 1974). Both methods are believed to create a textured surface, and alignment occurs from minimization of elastic strain in the nematic (Berreman 1972). When the instability is induced, the roll axis is always perpendicular to the director orientation, even if the applied voltage is uniform. We select the roll axis to be parallel to the electrode fingers. For all of the results except those presented in §5.3, the surface treatment was a rubbed polymer coating.

The glass plates are mounted on to two rigid steel plates whose spacing is controlled by three differential micrometers. This arrangement allows the layer depth, and hence the natural roll size, to be varied with a resolution of about a micron over the range 20–150 μm. The entire arrangement rests on the translation stage of a microscope and is maintained at a constant temperature of 20.0 ± 0.5 °C.

2.3. *Experimental procedure*

The patterns are studied as a function of two parameters. The first is the 'unperturbed' roll size $\frac{1}{2}l_0$ that is obtained in the absence of periodic forcing. (The width of two rolls is l_0, the period of the instability.) The roll size is varied between 20 and 150 μm by adjusting the layer thickness. It can be determined by Fourier analysis of data

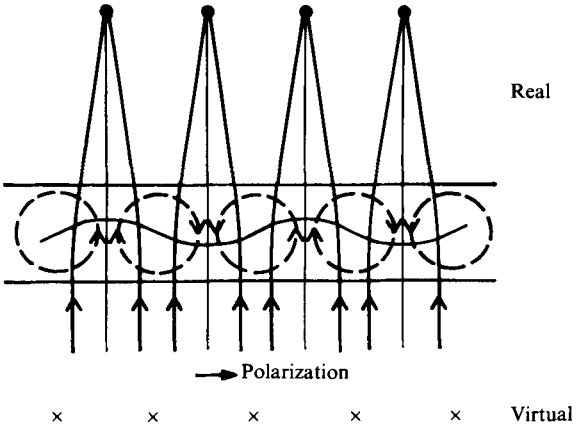

FIGURE 3. Schematic diagram of the EHD instability and its optical properties. An electric field applied across the fluid layer induces a flow pattern (dashed lines) similar to Rayleigh–Bénard convection. The director orientation varies sinusoidally. Incoming polarized light is focused by the layer to form real images above the cell and virtual images, designated underneath by ×. We observe the real images.

obtained from a region of the sample where the applied field is uniform. (Starting from V_c, the voltage is increased by increments of a few hundredths of a volt over a period of 1–2 h to avoid the formation of dislocations in the roll pattern.)

The second parameter is the strength of the periodic forcing, which we define in the following way. The two slightly different a.c. voltages (50 Hz), applied to the two parts of the lower electrode are always greater than the threshold V_c (≈ 6 V r.m.s.) for the onset of the EHD instability, but less than $1.12 V_c$. The mean distance above threshold, specified by $\epsilon = (V_{av} - V_c)/V_c$, where $V_{av} = \frac{1}{2}(V_A + V_B)$, is held constant. The forcing strength is then defined as the normalized difference $\alpha = |V_A - V_B|/V_c$.

The system is initially maintained at $\alpha = 0$ for about an hour in order to obtain a sample that is essentially unmodulated and free of dislocations. (However, there are effects due to a small residual forcing at $\alpha = 0$; these will be discussed later.) Then α is usually increased by small increments every 15–30 min, an interval sufficiently long that the patterns may reach a steady state. All of the patterns presented in this paper are essentially time-independent.

2.4. *Imaging and data analysis*

The flow is easily observed by polarized transmission microscopy, since the variable director orientation and anisotropy in the index of refraction give rise to strong refraction (see figure 3). Above the layer, light is focused by the nematic to form a bright line at each roll boundary (Penz 1971). (Virtual images are formed below the layer, and are displaced horizontally from the real images by half a roll.)

The patterns are recorded on videotape using a vidicon camera mounted on the microscope. Images are later digitized from the tape with a resolution of 320×240 pixels and 8-bit accuracy in the light-intensity levels.

In order to obtain accurate roll-position measurements, we average the signal from many video frames to reduce noise. To locate the roll boundaries, parabolic fits are applied to the maxima of the light intensities. Wavenumber measurements are also obtained by computing one- and two-dimensional Fourier transforms of the light-

intensity profiles with standard FFT methods. After squaring, the resulting power spectra are displayed on a graphics monitor and analysed interactively. In some cases power spectra from different parts of the sample are averaged to reduce noise.

3. Theoretical Background

The effects of spatially periodic forcing in thermal convection were first addressed theoretically by Kelly & Pal (1978) and by Pal & Kelly (1978, 1979). The forcing was introduced through either spatially periodic variations in the temperature at the boundaries, or a periodically varying layer depth. They explored the nature of the bifurcation to the convecting state using linear stability analysis, for various ratios of the forcing wavenumber k_1 to the critical wavenumber k_0. The threshold was found to be modified in most cases. The analysis specifically considered both uniform roll solutions, and three-dimensional superpositions of obliquely oriented rolls. The latter were found to have a lower bifurcation threshold than the two-dimensional structures in many cases, implying that three-dimensional convection can arise from two-dimensional spatial forcing.

Effects due to competing periodicities occur in many solid-state systems. For example, atoms adsorbed on a solid crystalline surface may form either commensurate or incommensurate patterns, depending on the relative sizes of the adsorbed and substrate atoms. The simplest model for this process, known as the Frenkel–Kontorova (FK) model (reviewed by Pokrovsky & Talapov 1984), turns out to be surprisingly relevant to the present hydrodynamic experiments. It consists of a chain of massive particles connected by springs, in the presence of a periodic potential. At the simplest level, the problem is to determine the equilibrium positions of the particles with respect to the potential. Although the model is discrete, Frank & van der Merwe (1949) discovered that in the limit of a weak sinusoidal potential, incommensurate states occur in which the displacements of the particles from the potential minima are described by continuous functions that are solutions to the sine-Gordon equation.

More recently, Aubry & André (1979) proved that both commensurate and incommensurate states of two distinct types occur in the FK model. The latter can be described in terms of a function $f(n\Lambda)$ defined for all n by

$$f(n\Lambda) = n\Lambda - x_n$$

where x_n denotes the position of the nth particle, Λ is the average spacing between the particles, and f is a periodic function with the period of the potential. At small forcing strengths, f is analytic, and the particle spacings vary gradually along the chain. On the other hand, when the forcing strength becomes sufficiently large, f may be discontinuous or non-analytic.

Amplitude equations, first introduced by Newell & Whitehead (1969) and Segal (1969), are widely used to understand the slow variations in space and time of a complex envelope or amplitude function $A(x,t)$ of the hydrodynamic fields. Since they arise from an expansion in powers and gradients of $A(x,t)$, they are useful only relatively near the onset of an instability. Motivated by preliminary results of the present investigation (Lowe & Gollub 1985*a*), Coullet (1986) showed that symmetry considerations uniquely specify the lowest-order contribution that periodic forcing makes to the amplitude equation:

$$A_t = \epsilon A - |A|^2 A + A_{xx} + \alpha (A^*)^{n-1} e^{inqx}.$$

The first four terms represent the form of the amplitude equation in the absence of spatial forcing. The quantity ϵ is the distance above onset; q is given by $k_1 = n(k_0+q)$ where n is an integer; and α is the forcing strength. The misfit q must be much smaller than k_0; this is the near-resonant forcing case.

The dynamics of this equation can be expressed in terms of a minimization principle. The quantity that is minimized is identical with the Hamiltonian of the FK model in the continuum limit. These results pertain to a range of parameters corresponding to weak forcing and small values of the misfit q. Thus, commensurate or phase-locked states occur, as well as incommensurate states in which the deviations of the roll positions from their commensurate values are correspondingly described by rotating solutions to the pendulum equation. The FK model, therefore, has some relevance to the present experiments even though it is not specifically hydrodynamic and does not include dissipation or diffusive relaxation.

Theoretical work using an amplitude-equation approach has also been presented by Lubensky & Ingersent (1986). They find that three-dimensional flows may be produced under certain circumstances when periodic forcing is present.

4. Commensurate states and the phase diagram

We explored the effects of external forcing by varying the forcing strength α and the ratio l_0/l_1 of periodicities. When α is non-zero, a variety of modulated structures appear. The simplest are the commensurate or phase-locked states, in which the period of the roll pattern is a multiple of l_1. The more complicated incommensurate states are discussed in §5.

4.1. *Low-order commensurate states*

Three low-order commensurate (C) states are seen in this experiment, corresponding to phase-locking at 1/1, 1/2 and 1/3. The notation m/n for the C-state indicates that n hydrodynamic periods ($2n$ rolls) occur in m periods of the forcing (a distance equal to ml_1). Photographs of several low-order ($m = 1$) commensurate states are presented in figure 4. (Not all of the sample is shown; the photographs illustrate only $\frac{1}{6}$ of the total sample area.) The electrode fingers are oriented vertically and are not directly visible. The centres of the convective rolls, which are parallel to the fingers, are represented by the dark stripes in the photos. The interaction between the natural period and the imposed one leads to perfect phase-locking over the entire interdigitated electrode. (The slight curvature in the rolls, noticeable in figure 4, is from photographing the patterns from a TV monitor. The rolls are straight in the digitized data.)

In order to exhibit the structure of the C-states, we present a graph of the transmitted light intensity across a C 1/3 pattern (see figure 5*a*). Each oscillation represents a single roll. There are six rolls for every period of the forcing, but not all of them correspond to the same light intensity. The graph is best described as a superposition of a slow oscillation at the forcing wavelength l_1, and a fast oscillation at an average wavelength of $l_1/6$. We believe that the underlying flow pattern may also be described by two superimposed roll structures with roll widths, l_1 and $l_1/6$.

The spatial structure may be understood more readily in the power spectrum, shown on a logarithmic scale in figure 5(*b*). The two dominant peaks are located at 49.4 ± 2.2 cm^{-1} ($\approx 1/l_1$) and 298.6 ± 2.5 cm^{-1} ($\approx 6/l_1$). The errors are obtained from the line widths of the peaks at half maximum. The proof that this pattern is commensurate comes from the fact that all peaks in the spectrum are located at

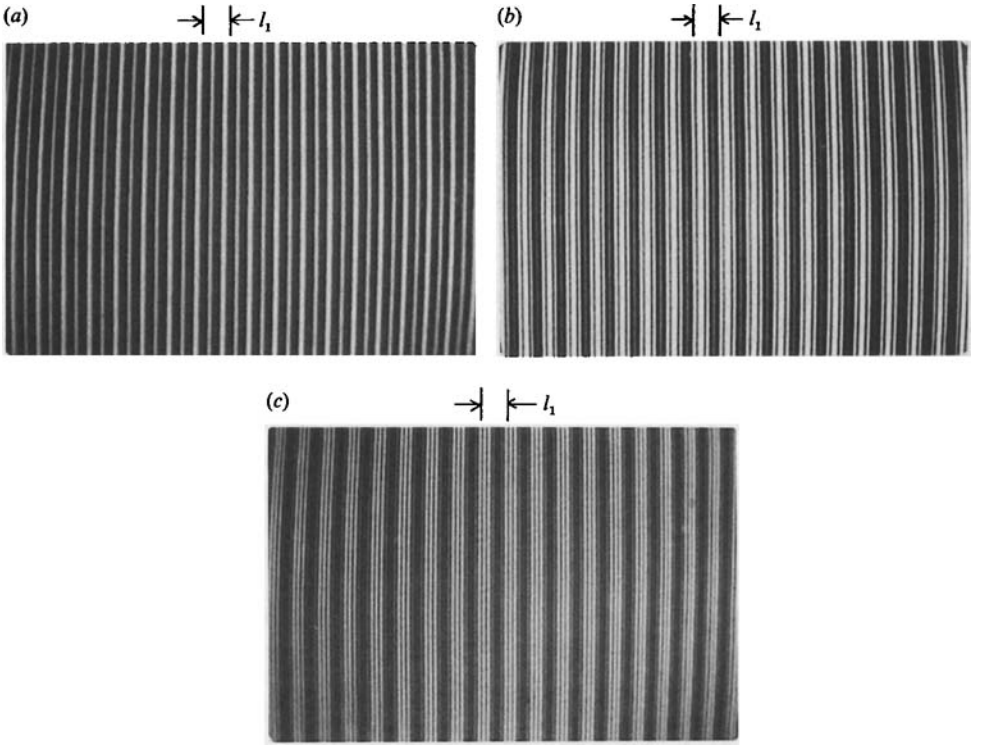

FIGURE 4. Low-order commensurate states. The convective rolls are aligned parallel to the fingers, which are not directly visible in the photos. (*a*) C 1/1 state for $l_0/l_1 = 0.928$ and $\alpha = 0.097$. (*b*) C 1/2 state for $l_0/l_1 = 0.460$ and $\alpha = 0.114$. (*c*) C 1/3 State for $l_0/l_1 = 0.370$ and $\alpha = 0.114$.

multiples of a single wavenumber; in this case, the fundamental component is k_1. (There is structure at $2k_1$, $3k_1$ and $5k_1$, but we do not have a quantitative understanding of it.)

4.2. *High-order commensurate states*

Two examples of high-order commensurate states are shown in figure 6; they correspond to phaselocking ratios of 2/3 and 2/5. In both cases the period of the pattern is $2l_1$. (In interpreting the photographs, recall that the roll width is the spacing between two bright stripes.) One distinction between these patterns and the low-order commensurate states (aside from the longer period) is the presence of domain walls, analogous to grain boundaries in a crystal. These walls separate commensurate regions, which are displaced by a multiple of l_1 relative to each other; in figure 6 the shift is exactly l_1.

In addition to the intensity variations, the C 2/5 pattern exhibits strong phase modulations in the roll positions with a period $2l_1$. We believe that this pattern can be best understood by a subgrouping of the pattern into alternating long (L) and short (S) 'blocks' consisting of 6 and 4 rolls respectively. The C 2/5 state can then be described (when grain boundaries are absent) by the sequence LSLSLS.... The average block size is l_1, but the ratio of the widths of the short and long blocks is 0.87. Thus the roll pattern in each group is similar to, but not exactly the same as, the low-order commensurate states 1/3 or 1/2. The importance of this subgrouping is described in more detail in §5.2.

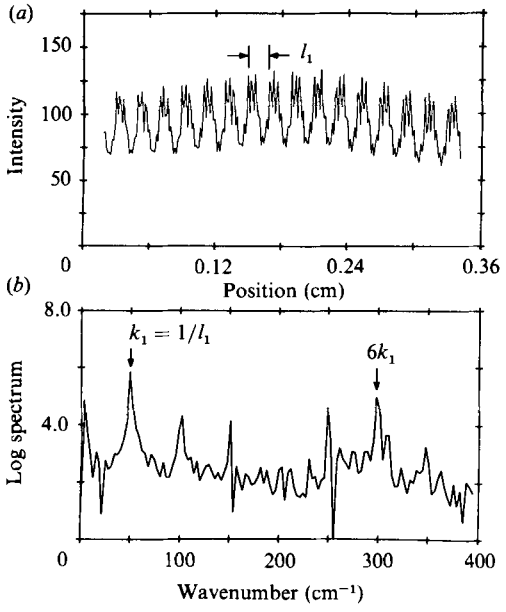

FIGURE 5. (*a*) Intensity profile of the C 1/3 state, shown in figure 4(*c*). The pattern is characterized by a slow modulation with period l_1 superimposed on a fast oscillation with period $l_1/6$. (*b*) Corresponding power spectrum. Two dominant wavenumbers appear at $k_1 = 1/l_1$ and $6k_1$, corresponding to the slow and fast oscillations. All other peaks in the power spectrum are located at multiples of k_1.

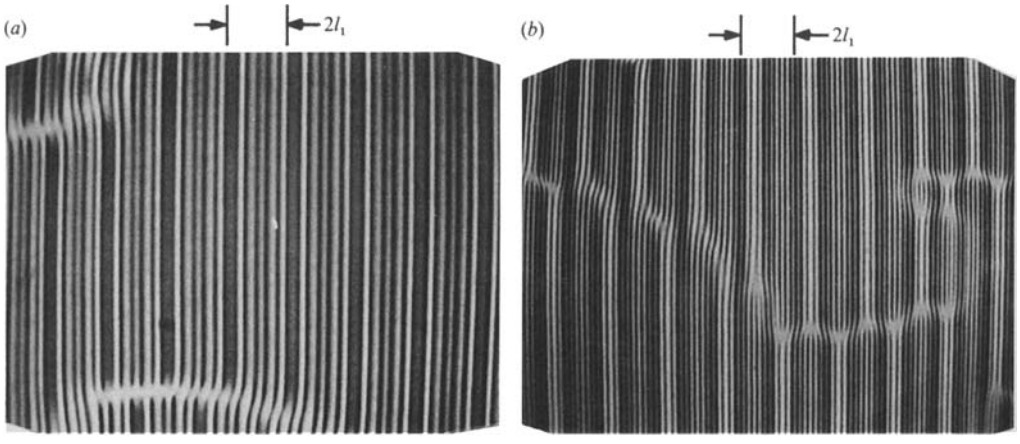

FIGURE 6. High-order commensurate states with grain boundaries. (*a*) *C* 2/3 state for $l_0/l_1 = 0.656$ and $\alpha = 0.114$. (*b*) C 2/5 state for $l_0/l_1 = 0.406$ and $\alpha = 0.081$. The structure may be subdivided into long and short blocks.

Other commensurate states were also noted, including C 5/14, 3/7, 3/8, 3/5 and 3/4. The locking is weak for these states, however, and the commensuration only extends over a few periods of the forcing. Defects and domain walls are prevalent in these patterns. Because of the limited spatial coherence, it is usually difficult to classify them unambiguously.

4.3. *Phase diagram*

The relationships among the commensurate states may be summarized in a phase diagram, shown in figure 7, for fixed $\epsilon = 0.057$. The vertical axis represents the strength of the forcing. The horizontal axis is the ratio l_0/l_1 of the two lengthscales. Based on several hundred data points, five commensurate regimes (shaded areas) are indicated in the graph, corresponding to C 1/1, 3/4, 2/3, 1/2 and 1/3. Except for the C 1/2 tongue, each region widens as α is increased; this is a sign of nonlinear coupling between the rolls and the forcing, leading to stronger phaselocking at larger values of α. Between the commensurate regions, incommensurate structures are found. The uncertainty in the position of the commensurate boundaries is approximately ± 0.01 horizontally. (In the blank region above the C 1/1 and 3/4 states, no observation was made.)

Certain commensurate states are not marked on the phase diagram, because they contain numerous defects. The most prominent omission is the C 2/5 state, located between the C 1/3 and 1/2 regions; more details are provided in §5.2. The other states are extremely narrow.

One surprising feature of the phase diagram is the non-zero width of the tongues at $\alpha = 0$: phase-locking occurs even when $V_A = V_B$. This is due to the finite width of the etched line that divides the two regions of the inter-digitated electrode. When $\alpha = 0$, this line causes the voltage near the surface of the electrode to be non-uniform. A calculation of the equipotential lines throughout the layer indicates that voltage variations near the surface are about 8% of V_A and have a period of 100 μm. This is comparable with typical values of $V_A - V_B$ and is evidently sufficient to cause commensuration at $\alpha = 0$. The C 1/2 and 1/1 tongues are affected most strongly. In fact, the C 1/2 tongue is broadest at $\alpha = 0$.

4.4. *Devil's staircase*

The organization of the commensurate states may also be presented at each value of α by a graph of the dominant periodicity of the modulated patterns as a function of l_0/l_1. One example is shown in figure 8 for $\alpha = 0.065$. The vertical axis represents (in units of l_1) the inverse l of the *mean* wavenumber of the modulated pattern, obtained from power-spectral measurements. In the figure, clear plateaux appear at $l/l_1 = 1.0$, 0.75, 0.5 and 0.33, corresponding to commensurate states at 1/1, 3/4, 1/2 and 1/3 respectively. Other commensurate states, such as C 2/5 and C 2/3, are obscured by the scatter in the plot, which is a consequence of the finite sample size. A graph of this type, with an infinite number of plateaux, is called a 'devil's staircase' (Aubry 1983).

The incommensurate states occur between the plateaux. We have studied the nature of the commensurate-to-incommensurate (C/I) transition for different values of the forcing strength. The clearest transition occurs near the C 1/1 state. For $\alpha = 0$ the variation of l with l_0 is smooth. As α is increased, the plateau at $l/l_1 = 1.0$ develops, but the variation of l with l_0 remains continuous. When $\alpha \gtrsim 0.05$, the curve becomes discontinuous at the step, and the amplitude of the jump increases with α. The onset of this discontinuity is shown by a point on the boundary of the C 1/1 state in the phase diagram (see figure 7). The change from a continuous to a discontinuous transition is analogous to a tricritical point in the study of phase transitions. Further discussion of the C/I transition may be found elsewhere (Lowe & Gollub 1985*a*).

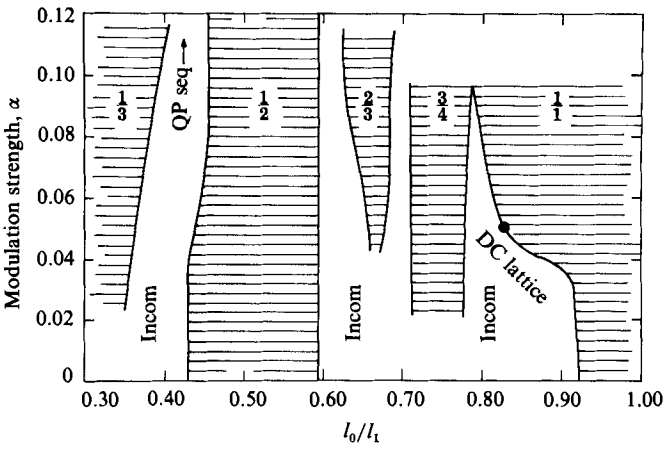

FIGURE 7. Phase diagram as a function of l_0/l_1 and the dimensionless modulation strength α for $\epsilon = 0.057$. The commensurate regions are represented by the shaded areas. The incommensurate regions are unshaded. Discommensurations (DC) and quasi-periodic sequences are found in certain incommensurate areas. The dot on the C 1/1 phase boundary is the point at which the C/I transition becomes discontinuous.

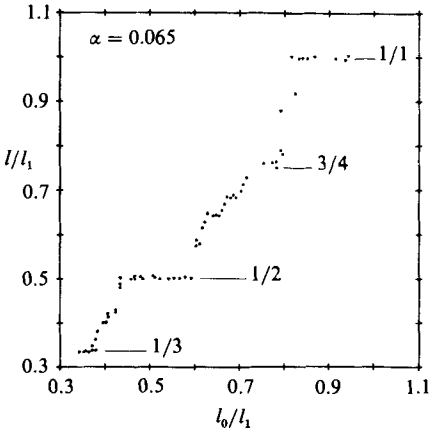

FIGURE 8. Variation of the inverse l of the mean wavenumber with the unperturbed roll size l_0 (in units of l_1) for $\alpha = 0.065$ and $\epsilon = 0.057$. Commensurate regions are represented by plateaux. Graphs of this type, with an infinite number of plateaux are called 'devil's staircases'.

5. Incommensurate states

Over large ranges of l_0/l_1, incommensurate patterns appear with structures characterized by amplitude and phase modulation of the rolls. To accommodate the forcing period, these states have a more complicated structure than the commensurate patterns described earlier. Three major types of incommensurate patterns are presented below. The first can be quantitatively described as a discommensuration lattice. The second appears to form quasi-periodic sequences described by a discontinuous hull function (defined in §3). The last is a three-dimensional flow with a lattice of kinks.

5.1. *Discommensuration arrays*

Incommensurate or quasi-periodic states containing discommensurations (see figure 9) are found over a substantial range in α and l_0 – for example between the 3/4 and 1/1 C phase boundaries, as shown in figure 7. Over most of the pattern, the

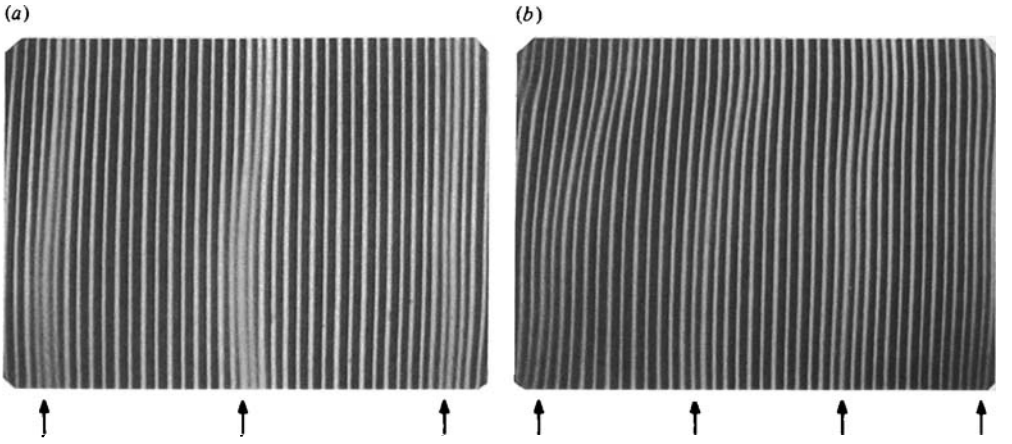

FIGURE 9. Incommensurate states characterized by discommensurations for $\alpha = 0.032$. (*a*) The discommensurations, indicated by arrows, are regions of compression of the rolls ($l_0/l_1 = 0.866$). (*b*) The discommensurations are more closely spaced. A defect in the upper left corner (not visible in the photograph) causes the lattice to shift towards the right ($l_0/l_1 = 0.816$).

rolls are nearly locked to the external forcing with a period similar to that of a C 1/1 pattern. Between these regions, the rolls are locally compressed. Figure 9(*a*) contains three compressed regions (marked by arrows); they may be called discommensurations. They are equally spaced and form a superlattice that is nearly parallel to the rolls. Another lattice, with more narrowly spaced discommensurations, is shown in figure 9(*b*). Sometimes such discommensurations are loosely described as solitons.

To exhibit the regions of compression quantitatively, we have studied these modulated patterns using digital image analysis. The size of each roll in figure 9(*a*) is shown in figure 10(*a*). The roll size varies periodically across the sample, nearly attaining the commensurate value of 100 μm in some regions. The areas of localized compression are the discommensurations. A phase variable $\phi(x_n)$ may be defined to denote the location x_n of the nth roll pair with respect to the external forcing:

$$\frac{\phi(x_n)}{2\pi} = \frac{x_n}{l_1} - n.$$

The phase is plotted as a function of position in figure 10(*b*). Each discommensuration corresponds to a phase change of 2π, or the insertion of an extra roll pair. Most of the phase change occurs over a distance that is small compared with the distance between the discommensurations, but large compared with l_0.

We noticed empirically that $\phi(x_n)$ may be closely approximated by rotating solutions $\phi(x)$ to the pendulum equation $\partial^2\phi/\partial x^2 = C \sin\phi$. Excellent nonlinear fits to the data can be constructed using these solutions:

$$\frac{\phi(x)}{2\pi} = a_1 - \frac{1}{\pi}\,\mathrm{am}\left(\frac{2K}{s}x + \delta\right),$$

where $\mathrm{am}(u)$ is the amplitude of an elliptic integral of the first kind (Milne-Thomson 1972). In this expression, s is the distance between the discommensurations, and K, a_1 and δ are constants. The minus sign is chosen to describe compression of the rolls. The solid line in figure 10(*b*) represents the nonlinear least-squares fit to our measured phase variation. We find that the data are quantitatively described by this function for $\alpha < 0.05$.

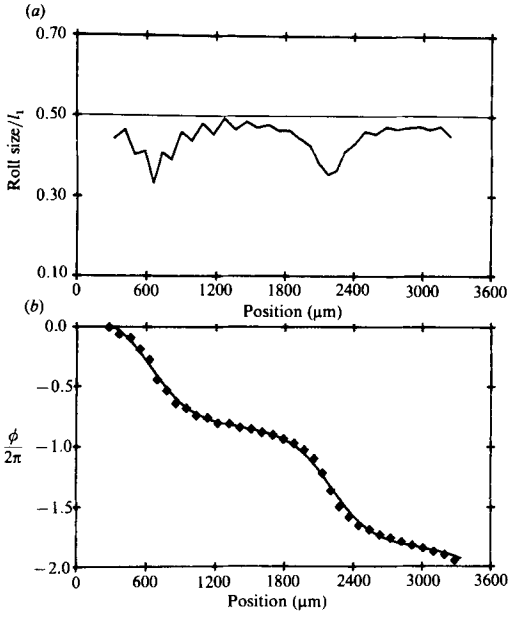

FIGURE 10. (*a*) Roll size (in units of l_1) across the sample shown in figure 9(*a*). Between the compressed roll regions, the pattern is nearly commensurate at 1/1. (*b*) Variation of the phase of the rolls across the sample. The solid line is a fitted solution to the pendulum equation, in which the best-fitting parameters are found to be: $a_1 = 0.66$; $K = 3.40$; $s = 1570$ μm; and $\delta = 5.23$ (see §5.1).

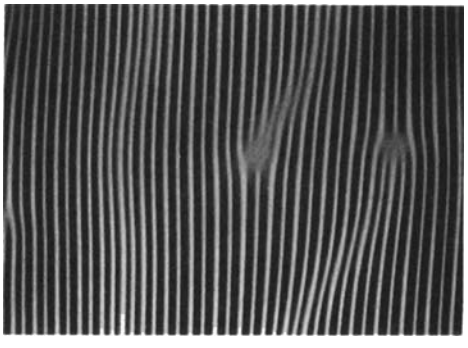

FIGURE 11. Photograph of a dislocation pair that leads to a defect in the discommensuration lattice.

Although most of the lattices are essentially two-dimensional, defects do occur. Sometimes the discommensurations are not strictly parallel to the rolls and terminate at dislocations in the roll pattern. An example of a dislocation pair is shown in figure 11. Another example is shown in the upper portion of figure 9(*b*), where a dislocation (not visible in the photograph) near the upper left corner causes the superlattice to shift towards the right. The spacing between the discommensurations remains constant except in the immediate vicinity of the defect.

5.2. *Quasi-periodic sequences*

Another type of incommensurate ordering was found at large values of α between the C 1/3 and 1/2 regions of the phase diagram of figure 7. Two examples at different

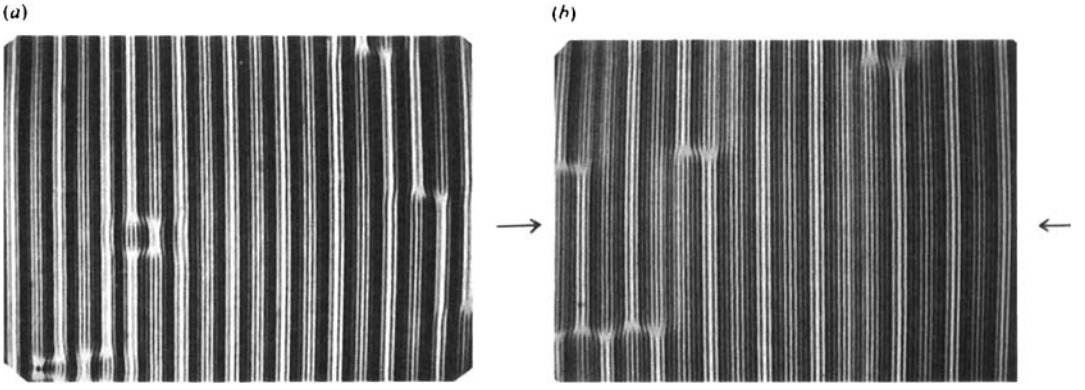

FIGURE 12. Quasi-periodic sequences characterized by long and short blocks. (*a*) A sequence with additional short blocks ($l_0/l_1 = 0.429$ and $\alpha = 0.114$). (*b*) A sequence with additional long blocks ($l_0/l_1 = 0.401$ and $\alpha = 0.081$). The sequence at the height of the arrows is LSLSLLSLSLSLLSLSLS.

values of l_0 are presented in figure 12. The rolls are strongly modulated by the forcing and are essentially parallel to the fingers of the interdigitated electrode. Large portions of both patterns resemble the C 2/5 state, shown in figure 6(*b*), in which the patterns may be subdivided into alternating long (L) and short (S) blocks consisting of 6 and 4 rolls respectively (see §4.2). The difference between the incommensurate patterns of figure 12 and the C 2/5 state is the insertion of extra L's or S's into the commensurate sequence LSLSLS in order to accommodate the pattern to the forcing. In figure 12(*a*), there are extra S's; in figure 12(*b*) there are extra L's. The average block size is still l_1.

We believe that these patterns are incommensurate, with a novel type of structure. To understand them, a slightly modified form of the hull function, mentioned in §3, is used, in which the particles correspond to *groups* of rolls. In this case, Λ is taken to be the average block size l_1, and the period of f is denoted Λ_f. To describe the data it is not possible for f to be continuous, since $x_{n+1}-x_n$ takes on only two discrete values: the width of either the long or short block. Lubensky suggested to us that f be a discontinuous periodic function, given by the expression

$$f(n\Lambda) = a\{n\Omega\}-\tfrac{1}{2}a.$$

Here a is a positive constant, and the function $\{n\Omega\}$ is defined to be equal to $n\Omega$ mod 1, where Ω is the ratio Λ/Λ_f. A graph of $f(n\Lambda)$ is shown in figure 13(*a*). Nonlinear functions with discontinuities are also possible.

With this choice for f, the expression for x_n (apart from a constant) may be more usefully written as

$$x_n = nS+(L-S)\,[n\Omega],$$

where L and S are the widths of the long and short blocks, and $[n\Omega]$ is the greatest integer less than or equal to $n\Omega$. The behaviour of $[n\Omega]$ is depicted graphically in figure 13(*b*) for the case $\Omega = 0.46$. For most successive values of n, the increase in $[n\Omega]$ alternates between 0 and 1. There are, however, occasions in which two adjacent zeros occur. This can be seen for $n = 16$ and 17. If Ω is irrational, then the sequence of 1's and 0's never repeats. Thus for values of Ω nearly equal to 0.5, the positions x_n increase by amounts generally alternating between L and S (see figure 13*c*). There are, however, occasional 'insertions' of either an S or an L.

This approach of using a discontinuous function to describe quasi-periodic patterns

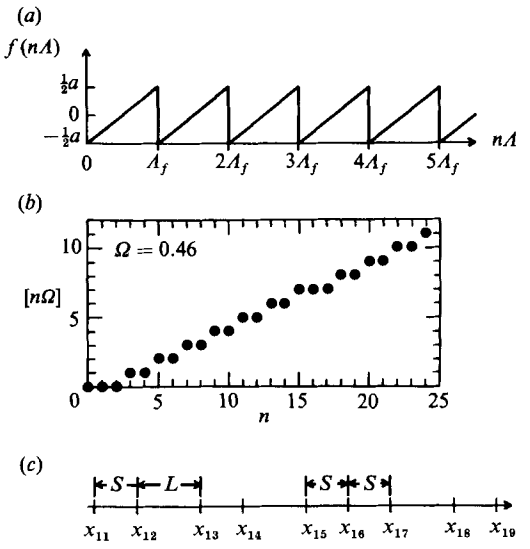

FIGURE 13. Explanation of the discontinuous function $f(n\Lambda)$ used to describe quasi-periodic sequences. (*a*) Graph of $f(n\Lambda) = a\{n\Lambda/\Lambda_f\} - \frac{1}{2}a$ versus $n\Lambda$. The function has a period Λ_f. (*b*) Graph of $[n\Omega]$ for $\Omega = 0.46$. This quantity usually increases by 1 for alternate values of n. However, at $n = 16$ and 17 (also $n = 2$ and 3), it fails to increase. (*c*) Sequence of long (L) and short (S) blocks corresponding to $\Omega = 0.46$.

may be applied to the data by converting the observed pattern into an array of 1's and 0's, as shown in figure 14(*a*). (The long and short blocks are represented by 1 and 0 respectively.) The solid lines indicate where there are two adjacent zeros. A number of dislocations are interspersed throughout the array, usually in pairs. Because of the dislocations, it is necessary to introduce a phase constant γ in applying the model to the experimental data: $x_n = nS + (L-S)[n\Omega + \gamma]$.

A large portion of the sample may be fitted by this equation. Each horizontal sequence in the right two-thirds of the array can be exactly reproduced, using a starting value of $n = 1$ and values of Ω near 0.46. The quantity γ is allowed to be different from line to line. A graph of Ω for each row is shown in figure 14(*b*). The bars indicate the range of Ω that is consistent with the data. The small variations in Ω over the pattern are probably due to the presence of slight inhomogeneities in the layer depth. This experimental limitation and the finite sample size leads to a somewhat inconclusive interpretation of the results. Nevertheless, the fits are successful enough that we consider these patterns to be incommensurate. This approach of using a discontinuous function to model the data is similar to recent efforts to describe certain incommensurate atomic arrays known as quasicrystals (Lubensky & Ingersent 1986).

5.3. *Three-dimensional flows*

The flows described up to this point are two-dimensional, except for the presence of defects. This is probably due to the oriented polymer coating that was applied to the electrodes to suppress three-dimensional effects. It is important to consider how the phenomena would be modified if no orientational preference is present. (Furthermore, one might ask what happens in an isotropic fluid.) If the polymer coating is simply eliminated, we find it is essentially impossible to produce an ordered array of rolls, because of apparently random variations in the director orientation. However, we

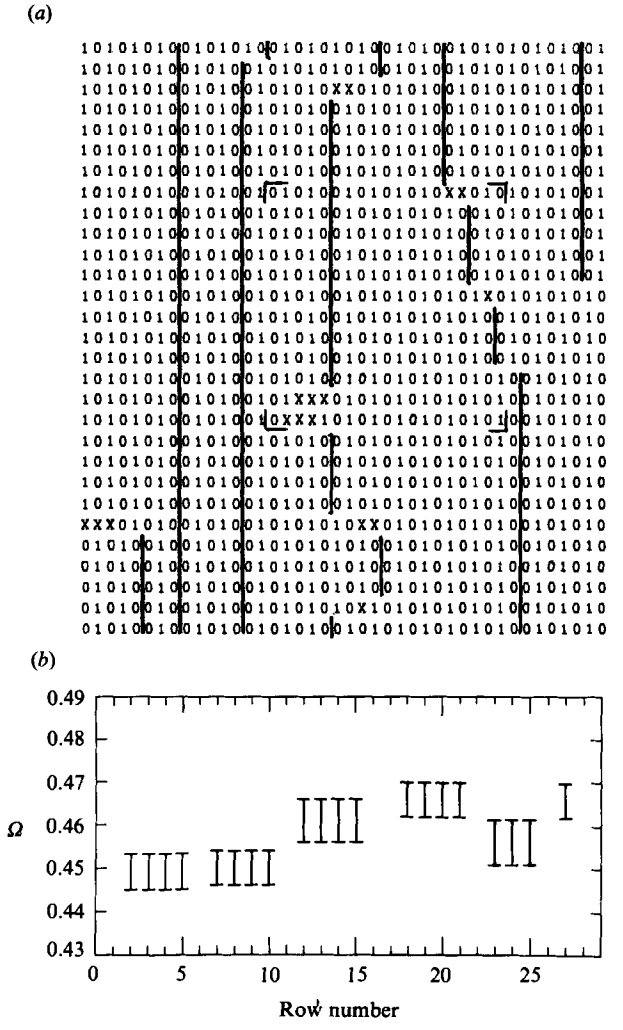

FIGURE 14. (*a*) Array of long (1) and short (0) blocks demonstrating possible quasi-periodic sequences. Figure 12(*a*) shows the region of the array within the brackets. The solid line separates two adjacent zeros, and the defects are marked with 'X'. (*b*) Fitted values of Ω for each horizontal sequence in the right two-thirds of the array. The brackets indicate the possible range of Ω. The variation in Ω with the pattern suggests that the layer depth is sligthly inhomogeneous.

did investigate the effect of an alternate method of surface treatment, based on an evaporated SiO film (see §2) that apparently produces a weaker orientational preference than does the polymer coating.

Over a wide range of roll sizes (84–116 μm) and forcing strengths, we found that the favoured structure is a three-dimensional flow, as shown in figure 15. (In this photograph, the electrode fingers are orientated at about 45° in the counterclockwise direction with respect to the vertical. Though this seems awkward, the computed two-dimensional power spectra are easier to interpret if major peaks do not lie along the coordinate axes.) The pattern still consists of rolls, but their dominant axis is rotated by an angle of $\theta = 19°$ with respect to the electrode fingers, which are parallel to the axis labelled y. The rolls now are modulated by a regular lattice of kinks where they cross the electrode fingers.

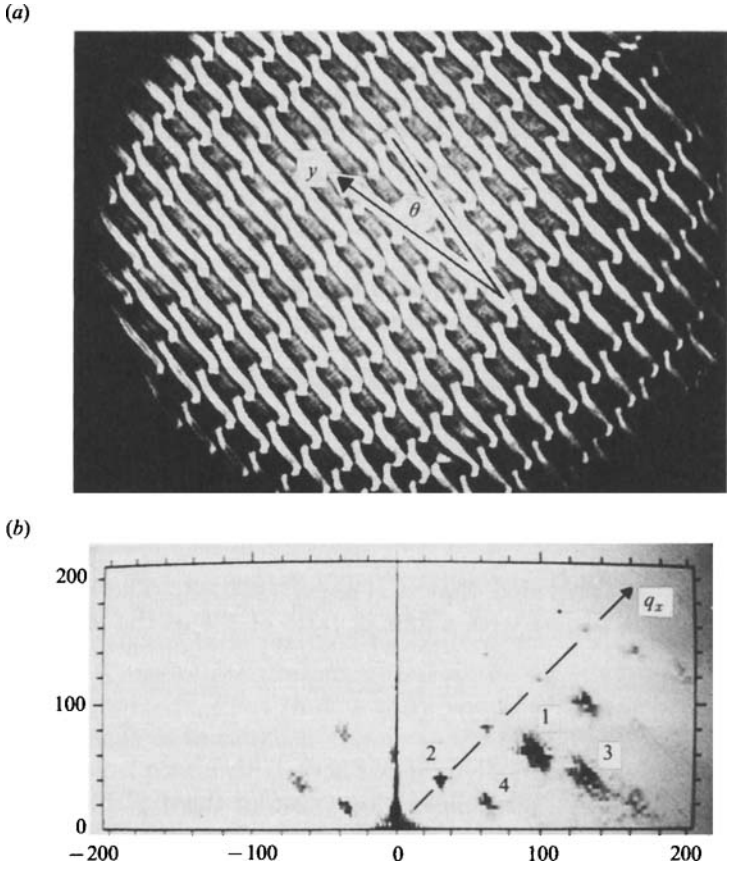

FIGURE 15. (*a*) Three-dimensional incommensurate structure with kinks ($l_0/l_1 = 0.91$). The electrode fingers are oriented along the (tilted) axis labelled y. However, the predominant roll orientation makes an angle $\theta = 19°$ with respect to y. (*b*) Corresponding two-dimensional power spectrum indicating that much of the power is off the q_x axis. The two dominant peaks are labelled 1 and 2, where 1 is the wavenumber of the rotated rolls, and 2 lies on the q_x axis and is due to the response of the system at the forcing wavenumber.

The computed two-dimensional spectrum (figure 15*b*) shows that the pattern is multiply periodic with two dominant wavevectors. The first of these is associated with the peak labelled 1. It corresponds to intensity variations perpendicular to the axis of the rotated rolls. The next largest peak (2) is located near the origin along the axis labelled q_x, and is a response due to the forcing with wavenumber $1/l_1$. More than 60 % of the total power falls under these two peaks. All peaks in the spectrum lie on a two-dimensional reciprocal lattice spanned by these two basis vectors.

In order to determine whether there is any kind of 'lock-in', we studied the wavenumber q' of the dominant off-axis peak (1) as a function of the wavenumber $2k_0$ of the unperturbed roll structure (see figure 16). This was accomplished by varying the layer thickness. We find no evidence of locking: q' varies smoothly with $2k_0$. Furthermore, the data points lie close to the line $q' = 2k_0$, indicating that the dominant periodicity is not much affected by the forcing; the primary means of accommodation to the perturbation is a rotation of the rolls. (Surprisingly, the rotation angle θ remains fairly constant at the value 20° over a range of k_0.)

Finally we note that similar three-dimensional flows appear in another parameter

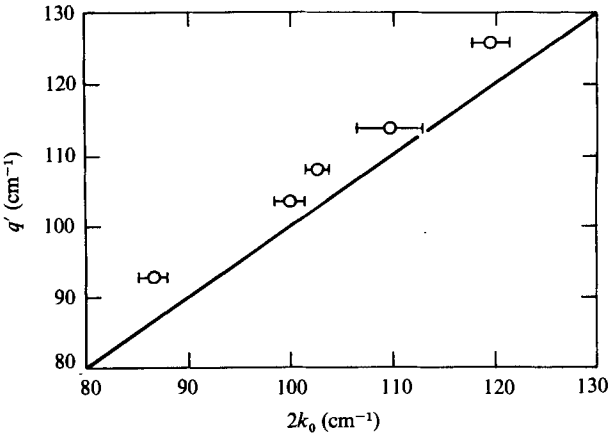

FIGURE 16. Variation of the wavenumber q' of the dominant off-axis peak with the unperturbed roll wavenumber $2k_0$. The data points lie close to the $q' = 2k_0$ line, indicating that the rolls mainly rotate as a result of the forcing.

range, $l_0/l_1 = 0.65$–0.70, provided that α is small (≈ 0.03). The rolls slowly align parallel to the electrode fingers with a lock-in ratio of 2/3 as the forcing strength is increased.

6. Discussion and conclusions

These experiments reveal a wide variety of flows with multiple periodicities in the presence of periodic forcing. We believe that most of these phenomena would be exhibited by ordinary Rayleigh–Bénard convection, though we have used an EHD instability for reasons given earlier. Even for thermal convection, it does not seem likely that direct solution of the hydrodynamic equations without approximation will be practical. On the other hand, many of our observations can be interpreted with the aid of amplitude equations.

Before discussing the observations, we point out that many important issues have not been addressed in these experiments. The predictions of Kelly & Pal (1978) and Pal & Kelly (1978, 1979) on the modification of the bifurcation by the forcing have not been tested. Also, our experiments have been confined to small ϵ, where the flows are time independent.

We note that the distinctions between commensurate and incommensurate states are sometimes difficult to make even with samples of several hundred rolls. Also, it is often impracticable to distinguish between defects and dislocations that would occur under ideal circumstances, and those that result from imperfect sample preparation (for example imperfect alignment of the director at the electrode), or from failure to wait sufficiently long.

Coullet's (1986) work shows that the amplitude-equation approach is capable of describing the simplest phase-locked commensurate state and the nearby incommensurate state. The latter is described quantitatively by a phase variable whose dependence on position is given by rotating solutions to the pendulum equation. The generality of this approach suggests that it should be applicable near the threshold of any instability yielding a spatially periodic flow. The physical quantities specific to each system do not affect the form of the amplitude equation.

Furthermore, we note that within the framework of the amplitude equation, stable

flows may be regarded as minimizing a certain potential. In this experiment, it has the same form as the Hamiltonian of the FK model in the continuum limit. The existence of such a potential for weak forcing near threshold is responsible for the close correspondence between the behaviour of this non-equilibrium system and analogous commensurate and incommensurate phenomena in statistical mechanics.

We believe that the three-dimensional flows (figure 15) can be explained by a suitable extension of the amplitude equation to two horizontal dimensions, as proposed by Lubensky & Ingersent (1986). These flows may also be related to the oblique-roll states of Pal & Kelly (1979). The basic physical reason for the three-dimensionality within the framework of the amplitude equation is that lower values of the potential can be reached if roll compression (or stretching) is avoided by taking advantage of the other horizontal dimension.

Unfortunately, the amplitude equation cannot explain all of the observations in these experiments. For example, the high-order commensurate phases, which have rapid spatial variations in the roll amplitudes and phases, cannot be predicted by Coullet's theory (or any approach involving amplitude equations). Their internal structure (figure 5) is not understood. Similarly, the incommensurate states that we model as quasi-periodic sequences described by a discontinuous function $f(n\Lambda)$ also cannot be treated by the basic amplitude equation. It remains to be seen whether the description given in §5.2, which is based on the behaviour of the discrete FK model, can be fundamentally justified for hydrodynamics. Certainly, other features similar to the FK model are present in our data: for example, the commensurate tongues in the phase diagram that usually widen as α increases, and the narrow high-order commensurate tongues.

In a separate investigation (Lowe & Gollub 1985*b*), we have utilized the experimental methods described in this paper to study the Eckhaus instability, in which a convective flow with wavenumber far from the critical value goes unstable with respect to long-wavelength modulations, yielding a transient flow having several periodicities. This phenomenon may be understood using amplitude equations.

We suggest that studies of the response of hydrodynamic systems to spatially periodic forcing can potentially yield surprises in addition to those presented here, because of the profound effect of altering the basic symmetry of the system. Much theoretical work remains to be done in attempting to understand these striking phenomena.

This work was supported by the National Science Foundation MRL program under DMR-8519059, and by the NSF Fluid Mechanics Program under MSM-8310933. We appreciate helpful discussions with P. Coullet and T. Lubensky.

REFERENCES

AUBREY, S. 1983 The twist map, the extended Frenkel–Kontorova model and the devil's staircase. *Physica D* **7**, 240–258.

AUBREY, S. & ANDRÉ, G. 1979 Analyticity breaking and Anderson localization in incommensurate lattices. *Annls Israel Phys. Soc.* **3**, 133–164.

BERREMAN, D. W. 1972 Solid surface shape and the alignment of an adjacent nematic liquid crystal. *Phys. Rev. Lett.* **28**, 1683–1686.

BUSSE, F. H. & WHITEHEAD, J. A. 1971 Instabilities of convection rolls in a high Prandtl number fluid. *J. Fluid Mech.* **47**, 305–320.

CHEN, M. M. & WHITEHEAD, J. A. 1968 Evolution of two-dimensional periodic Rayleigh convection cells or arbitrary wave-numbers. *J. Fluid Mech.* **31**, 1–15.

COULLET, P. 1986 Commensurate–incommensurate transitions in non-equilibrium systems. *Phys. Rev. Lett.* **56**, 724–727.

FRANK, F. C. & VAN DER MERWE, J. H. 1949 One-dimensional dislocations. *Proc. R. Soc. Lond.* A **198**, 205–225.

GOOSSENS, W. J. A. 1978 Electrohydrodynamic instabilities in nematic liquid crystals. In *Advances in Liquid Crystals* (ed. G. H. Brown), pp. 1–39. Academic.

KELLY, R. E. & PAL, D. 1978 Thermal convection with spatially periodic boundary conditions. *J. Fluid Mech.* **86**, 433–456.

LOWE, M. & GOLLUB, J. P. 1985*a* Solitons and the commensurate–incommensurate transition in a convecting nematic fluid. *Phys. Rev.* A **31**, 3893–3897.

LOWE, M. & GOLLUB, J. P. 1985*b* Pattern selection near the onset of convection: the Eckhaus instability. *Phys. Rev. Lett.* **55**, 2575–2578.

LOWE, M., GOLLUB, J. P. & LUBENSKY, T. 1983 Commensurate and incommensurate structures in a nonequilibrium system. *Phys. Rev. Lett.* **51**, 786–789.

LUBENSKY, T. C. & INGERSENT, K. 1986 Patterns in systems with competing incommensurate lengths. In *Proc. NATO Advanced Research Workshop on Patterns, Defects, and Microstructures in Non-Equilibrium Systems* (ed. L. Reichl). Martinus Nijhoff, (to appear).

MILNE-THOMSON, L. M. 1972 Jacobian elliptic functions and theta functions; also elliptic integrals. In *Handbook of Mathematical Functions* (ed. M. Abramowitz & I. A. Stegun), pp. 567–626. Dover.

NEWELL, A. C. & WHITEHEAD, J. A. 1969 Finite bandwidth, finite amplitude convection. *J. Fluid. Mech.* **38**, 279–303.

PAL, D. & KELLY, R. E. 1978 Thermal convection with spatially periodic nonuniform heating: nonresonant wavelength excitation. In *Proc. 6th Intl Heat Transfer Conference*, vol. 2, pp. 235–238. National Research Council of Canada.

PAL, D. & KELLY, R. E. 1979 Three-dimensional thermal convection produced by two-dimensional thermal forcing. In *Proc. Joint ASME/AIChE 18th National Heat Transfer Conference*, paper 79-HT-109. American Society of Mechanical Engineers.

PENZ, P. A. 1971 Order parameter distribution of the electrohydrodynamic mode of a nematic liquid crystal. *Molec. Crystals and Liquid Crystals* **15**, 141–160.

POKROVSKY, V. L. & TALAPOV, A. L. 1984 *Theory of Incommensurate Crystals.* Harwood.

SEGEL, L. A. 1969 Distant side-walls cause slow amplitude modulation of cellular convection. *J. Fluid. Mech.* **38**, 203–224.

URBACH, W., BOIX, M. & GUYON, E. 1974 Alignment of nematics and smectics on evaporated films. *Appl. Phys. Lett.* **25**, 479–481.